Ultrasonics - Sonochemistry 40 (2018) 900–911

Contents lists available at ScienceDirect

Ultrasonics - Sonochemistry

journal homepage: www.elsevier.com/locate/ultson

Bubble dynamics in viscoelastic soft tissue in high-intensity focal ultrasound thermal therapy

E. Zilonova[a], M. Solovchuk[a,d,*], T.W.H. Sheu[a,b,c]

[a] Department of Engineering Science and Ocean Engineering, National Taiwan University, No. 1, Sec. 4, Roosevelt Road, Taipei 10617, Taiwan, ROC
[b] Center of Advanced Study in Theoretical Science (CASTS), National Taiwan University, Taiwan, ROC
[c] Department of Mathematics, National Taiwan University, Taiwan, ROC
[d] Institute of Biomedical Engineering and Nanomedicine, National Health Research Institutes, No. 35, Keyan Road, Zhunan 35053, Taiwan, ROC

ARTICLE INFO

Keywords:
Cavitation in soft tissue
Gilmore-Akulichev model
Zener viscoelastic model
High–intensity focused ultrasound
Heat deposition

ABSTRACT

The present study is aimed to investigate bubble dynamics in a soft tissue, to which HIFU's continuous harmonic pulse is applied by introducing a viscoelastic cavitation model. After a comparison of some existing cavitation models, we decided to employ Gilmore-Akulichev model. This chosen cavitation model should be coupled with the Zener viscoelastic model in order to be able to simulate soft tissue features such as elasticity and relaxation time. The proposed Gilmore-Akulichev-Zener model was investigated for exploring cavitation dynamics. The parametric study led us to the conclusion that the elasticity and viscosity both damp bubble oscillations, whereas the relaxation effect depends mainly on the period of the ultrasound wave. The similar influence of elasticity, viscosity and relaxation time on the temperature inside the bubble can be observed. Cavitation heat source terms (corresponding to viscous damping and pressure wave radiated by bubble collapse) were obtained based on the proposed model to examine the cavitation significance during the treatment process. Their maximum values both overdominate the acoustic ultrasound term in HIFU applications. Elasticity was revealed to damp a certain amount of deposited heat for both cavitation terms.

1. Introduction

High intensity waves propagating through the medium may lead to the formation of cavities, which can be filled with gas or vapor. This effect is known as acoustic cavitation. Early studies on acoustic cavitation were mainly focused on different hydrodynamics applications [1], starting from work of [2]. Later, Plesset [3] constructed the mathematical model, which is called Rayleigh-Plesset equation, and still remains the most popular cavitation model for the description of single bubble oscillations in a liquid. Recently, the interest in cavitation has been growning due to different biomedical applications, mainly biomedical imaging and therapeutic ultrasound. In biomedical imaging, bubble-based contrast agents are successfully used to improve the image quality [4,5]. Theoretical and experimental study on cavitation effects in biomedical imaging has been mainly performed for safety reasons (with application of low intensity ultrasound).

With the increase of intensities, ultrasound can be applied for many therapeutic applications, such as non-invasive treatment of tumors in different parts of the body, arterial occlusion and acoustic hemostasis, treatment of neurological disorders and gene delivery [6–9]. Thermal and mechanical mechanisms can contribute to the treatment. It was shown [10,11] that cavitation effects can enhance energy deposition during thermal therapy, although appearance of cavitation makes the treatment less predictable. Without microbubbles, the necrosed area has a defined ellipsoidal shape and can be well predicted based on the Penne's bioheat equation [12,11,13]. Some therapeutic modalities, such as lithotripsy [14,15] and histotripsy [16,17], rely mainly on cavitation effects. However, at the present moment, it is not very clear, which thermal, mechanical and bio-effects of cavitation play the main role during different therapeutic applications. In order to understand them better and improve the treatment, fundamental understanding is necessary.

In the present work, we have developed the mathematical model for the description of the bubble oscillations that can be applied at high ultrasound intensities, in viscoelastic medium with relaxation and at high ultrasound frequencies. Both cavitation model for bubble dynamics and viscoelastic model are crucial for the accurate description of bubble collapse and understanding of bubble behavior in different biological tissues. For the better understanding of thermal effects, the bioheat equation will be presented with cavitation effects taken into account.

Nowadays, various cavitation models exist. Rayleigh-Plesset (RP,

* Corresponding author at: Institute of Biomedical Engineering and Nanomedicine, National Health Research Institutes, No. 35, Keyan Road, Zhunan 35053, Taiwan, ROC.
E-mail addresses: zilorina@mail.ru (E. Zilonova), solovchuk@gmail.com, solovchuk@nhri.org.tw (M. Solovchuk), twhsheu@ntu.edu.tw (T.W.H. Sheu).

http://dx.doi.org/10.1016/j.ultsonch.2017.08.017
Received 15 May 2017; Received in revised form 4 August 2017; Accepted 18 August 2017
Available online 19 August 2017
1350-4177/

[2]) model has been widely used due to its simplicity. The main assumption that distinguishes this model from others is to treat liquid as an incompressible fluid, which leads to the unphysical speed of sound equal to infinity. Another drawback of this model is that it is valid only at small Mach numbers $\frac{\dot{R}}{c} \ll 1$. In order to correct speed of sound in Rayleigh-Plesset model, Herring-Trilling (HT, [18,19]) and Keller-Miksis (KM, [20–22]) models were proposed that consider a liquid as a compressible fluid. Thus, the speed of sound is constant in both HT and KM models. That results in taking into account acoustics damping effect: in as much as when bubble oscillates in a compressible fluid, it acts as a source for wave generation. Modified Herring-Trilling model (MHT, [23]), sometimes called modified Rayleigh-Plesset model) is regarded as an intermediate model in between RP model and HT model: it retains the simplicity of RP model, but includes an essential acoustic damping term as in HT model. However, all mentioned acoustic damping models (HT, KM, MHT) can be applied only for Mach numbers not larger than 1. Nevertheless, at high acoustic pressures of incident focused ultrasound, Mach number can exceed this number. Gilmore-Akulichev [24] model solves this problem and, therefore, goes further than Herring-Trilling and Keller-Miksis models: it considers the pressure dependent speed of sound and is suitable for the conditions with high Mach number (because the speed of the bubble wall is deemed to be comparable to the speed of sound). The present study will be focused on the Gilmore-Akulichev model that has been considered as the most developed and realistic cavitation model, since it well describes the bubble collapse situation that is associated with high Mach numbers.

Most of the early studies on cavitation have been performed in liquids for Newtonian fluids [1]. However, soft tissues can not be considered as Newtonian fluids, since it is essential to take into account soft tissue's properties such as elasticity. Therefore, the employed cavitation model should be combined with one of the viscoelastic models. Up to the present moment, diverse models for describing viscoelastic medium exist and plenty of them were investigated in coupling with one of the cavitation models. Tanasawa and Yang [25] used Rayleigh-Plesset equation together with Jeffreys model as a viscoelastic model. Yang and Church [26] employed Keller-Miksis equation coupled with the Kelvin-Voigt viscoelastic model. Gaudron, Warnez and Johnsen [27] extended the approach of Yang and Church by considering a Neo-Hookean model for modeling the finite-deformation elasticity in an elastic term of Kelvin-Voigt model with Keller-Miksis equation. Movahed [28], as well, considered Kelvin-Voigt model, but it was coupled with Modified Herring-Trilling equation (called as the modified Rayleigh-Plesset model in their paper). Warnez and Johnsen [29] provided a nice review of the existing viscoelastic models: Kelvin-Voigt, Zener, Jeffreys, Maxwell, Oldroyd models on the basis of Keller-Miksis equation. However, the above mentioned models are based on RP, HT, KM equations, which can be applied only at low ultrasound intensities and at low Mach numbers, as we mentioned before. Brujan [30,31] investigated Rayleigh-Plesset, Herring-Trilling, Keller-Miksis, Gilmore-Akulichev and his own model, which were coupled with Oldroyd and Maxwell viscoelastic models.

Not all existing viscoelastic models are employed for describing soft tissue behavior. In literature, usually Maxwell, Kelvin-Voigt and Zener models are used for these purposes. Kelvin-Voigt model effectively describes the creep behavior of tissue, whereas Maxwell model effectively describes the relaxation process, but Catheline [32] showed that for modeling a soft tissue, Kelvin-Voigt model is superior to the Maxwell model. Focused ultrasound transducers are usually operated at MHz frequencies, which means that the period of the wave is of the order of microsecond. At such small periods, relaxation processes in tissues become important, because relaxation time can be comparable to the period of the wave. In [33], it was shown that at high intensities relaxation effects can significantly affect the amount of ultrasound energy deposited to the tumors. Therefore, both relaxation and elasticity should be taken into account for the modeling of bubble oscillations during HIFU therapy. Zener model is one of the simplest viscoelastic models that accounts for relaxation and elasticity at the same time. Zheng et al. [34], Suomi et al. [35] consider Zener model as the one that describes soft tissues in a more accurate way than Maxwell and Kelvin-Voigt models do (various soft tissues with Zener model were modeled in [36]). Moreover, Maxwell and Kelvin-Voigt models are just the limiting cases of Zener model. Thus, for the current simulations, our main focus would be placed on Zener model, since it is capable of describing both of general tissue features (namely, elasticity and relaxation time), and is considered to be more precise in predicting tissue viscoelastic behavior.

In order to understand the cavitation significance in the treatment process, the heat deposition in tissue generated by the acoustically driven bubbles should be investigated. Tumor ablation is a result of tissue heating, caused by conversion of HIFU's energy into thermal energy. Cavitation is implicated to this process and can elevate tissue's temperature. Therefore, it is essential to estimate the order of obtained thermal energy values that correspond to the cavitation's contribution. Tissue heating is well described by Pennes's bioheat transport equation. To take into account the cavitation heating, extra source terms should be added to the original equation. Bubble can convert acoustic energy into thermal energy in three ways: thermal damping, viscous damping and absorption of the radiated pressure wave induced by bubble collapse [37]. However, several authors [38–41] etc. have demonstrated that the contribution of thermal damping term is minimal. Therefore, in the present study we consider only two extra source terms in BHTE corresponding to the heating induced by cavitation and perform the related calculation.

This manuscript is organized as follows. First, the comparison of the Gilmore-Akulichev model with other cavitation models is shown. Next, the new proposed Gilmore-Akulichev-Zener model is described. Then the parametric study based on this model is performed together with the predicted numerical results. Further on, the calculation of the temperature within the bubble is performed. Finally, the study of the heat deposition caused by cavitation is presented.

2. Existing cavitation models

2.1. Limitations on some existing cavitation models

Authors considered Rayleigh-Plesset, Herring-Trilling, Modified Herring-Trilling, Keller-Miksis and Gilmore-Akulichev cavitation models. Peculiarities of these models are summarized in Table 1. It can

Table 1
Comparison of investigated cavitation models.

Rayleigh-Plesset	Modified Herring-Trllling	Herring-Trilling	Keller-Miksis	Gilmore-Akulichev
Incompressible liquid, infinite speed of sound	Compressible fluid, constant finite speed of sound			Compressible fluid, pressure dependent speed of sound
No damping in acoustic radiation	Damping resulting from acoustic radiation			
$\frac{\dot{R}}{c} \ll 1$		$\frac{\dot{R}}{c} < \frac{1}{2}$	$\frac{\dot{R}}{c} < 1$	$\frac{\dot{R}}{C} < 2.2$
Driving acoustic pressure $p_i(t)$ is included as an input to background pressure p_0			Driving acoustic pressure $p_i(t)$ is included explicitly in derivation	Driving acoustic pressure $p_i(t)$ is included as an input to background pressure p_0

be seen that even though Rayleigh-Plesset model is relatively simple, however, it has such a serious drawback as not taking into account the acoustic damping (because of treating liquid as incompressible fluid) that can greatly affect the bubble dynamics (as can be seen below in simulations). Modified Herring-Trilling model overcomes this drawback by including an acoustic damping term. However, it's range of applicability is still quite limited as for the Rayleigh-Plesset. The Herring-Trilling and Keller-Miksis models were later developed considering compressible liquid and, hence, the acoustic damping. Prosperetti [42] has shown that the difference between these two models is the presence of the second order term of $\dot{R}/c$, thus, these models are very similar. Inclusion of the driving pressure $p_i(t)$ explicitly in Keller-Miksis model does not make a significant effect comparing to other models. It can be seen that the Keller-Miksis's application range is slightly larger than the one for Herring-Trilling – this could be the only reason to give a preference to Keller-Miksis. Gilmore-Akulichev still considers acoustic damping, but, also, accounts for the pressure dependent speed of sound. The description of a more realistic effect and the applicability for high Mach numbers are the compelling advantages that can urge one to employ Gilmore-Akulichev model in simulations.

2.2. Gilmore-Akulichev equation

In what follows, we denote $R(t)$ – radius of the bubble, p – tissue pressure on the bubble wall, p_∞ – far-field pressure, ρ – tissue density, μ – tissue viscosity, S – surface tension, c – speed of sound, h – tissue enthalpy, u – tissue velocity, r – the distance from the center of bubble, Φ – tissue's velocity potential, τ_{rr} – stress in a motion in r direction, R_0 – initial bubble radius.

Gilmore model employs the diverging wave equation $\left(\frac{\partial}{\partial t}+c\frac{\partial}{\partial r}\right)(r\Phi)=0$, which has the solution cast in the following form:

$$\Phi=\frac{f\left(t-\frac{r}{c}\right)}{r} \tag{1}$$

Bernoulli equation can be written as follows with Eq. (1) being considered:

$$r\left(h+\frac{1}{\rho}\int_r^\infty\left(\frac{\partial\tau_{rr}}{\partial r}+\frac{3\tau_{rr}}{r}\right)dr+\frac{u^2}{2}\right)=f'\left(t-\frac{r}{c}\right) \tag{2}$$

For Gilmore-Akulichev's model in [24], the assumption that $r\Phi$ propagating with the velocity $c+u$ (c is local sound velocity) is applied, instead of habitual quasi-acoustic assumption that the propagation velocity is c_∞ (as in Herring-Trilling and Keller-Miksis). This assumption should be made in order to describe the situation, when liquid velocities attain an appreciable fraction of the sound velocity. After a further derivation, Gilmore-Akulichev's model has the following form:

$$R\ddot{R}\left(1-\frac{\dot{R}}{C}\right)+\frac{3}{2}\dot{R}^2\left(1-\frac{\dot{R}}{3C}\right)= \tag{3}$$

$$H\left(1+\frac{\dot{R}}{C}\right)+\frac{R\dot{H}}{C}\left(1-\frac{\dot{R}}{C}\right)+$$
$$+\left(1+\frac{\dot{R}}{C}\right)\left(\frac{1}{\rho}\int_R^\infty\left(\frac{\partial\tau_{rr}}{\partial r}+\frac{3\tau_{rr}}{r}\right)dr\right)+ \tag{4}$$

$$+\frac{R}{C}\frac{d}{dt}\left(\frac{1}{\rho}\int_R^\infty\left(\frac{\partial\tau_{rr}}{\partial r}+\frac{3\tau_{rr}}{r}\right)dr\right), \tag{5}$$

Here H and C denote respectively the values of enthalpy and sound speed at the bubble wall [24] states that for most of the liquids the pressure-density curve for an isentropic compression can be well fitted by the formula $\frac{p+B}{p_\infty+B}=\left(\frac{\rho}{\rho_\infty}\right)^n$):

$$H=\frac{1}{\rho}\frac{n}{n-1}(p_\infty+B)\left(\left(\frac{p+B}{p_\infty+B}\right)^{\frac{n-1}{n}}-1\right),$$
$$C=c_\infty\left(\frac{p+B}{p_\infty+B}\right)^{\frac{n-1}{2n}}, \tag{6}$$

where B and n are particular liquid constants that were set for tissue accordingly to [40].

Far-field pressure p_∞ can be considered as a sum of the static background pressure p_0 and the varying driving sound field $p_i(t)$.

Viscous and surface tension forces can strongly affect the bubble surface. As a result, it makes sense to take them into consideration as pressure boundary conditions at the bubble surface. With the surface tension term being considered in the form of $\frac{2S}{R}$ (Laplaces's formula), the equation for the pressure at the interface is:

$$p=p_G\left(\frac{R_0}{R}\right)^{3\gamma}-\frac{2S}{R}+\tau_{rr}|_{r=R} \tag{7}$$

Eq. (5) covers a velocity range extending to $\frac{\dot{R}}{C}=2.2$ [24], implying that Gilmore-Akulichev model has the largest applicability range. It is, therefore, suitable for the situations involving large amplitudes [43].

3. Zener viscoelastic model

Zener viscoelastic model [44] can be represented as a spring (with rigidity G_2) in series with a dashpot (with viscosity ν) and in parallel with another spring (with elasticity G_1) – Fig. 1.

With tissue parameters defined as the relaxation time $\lambda_1=\frac{\nu}{G_2}$, rigidity $G=G_1$ and viscosity $\mu=\frac{\nu}{G_2}(G_1+G_2)$, Zener model can be written as:

$$\tau_{rr}+\lambda_1\dot{\tau_{rr}}=2G\gamma_{rr}+2\mu\dot{\gamma_{rr}}, \tag{8}$$

where γ_{rr} is a strain and $\dot{\gamma_{rr}}$ is a strain rate. For both compressible and incompressible cases, strain rate equals $\dot{\gamma_{rr}}=-2\frac{R^2\dot{R}}{r^3}$ (derived from continuity equation while neglecting terms of the order of c^{-2}). The strain turns out to be $\gamma_{rr}=-\frac{2}{3r^3}(R^3-R_0^3)$.

There are two limiting cases for the Zener model: with $\lambda_1=0$, Zener model reduces to the Kelvin-Voigt model and, when $G=0$, Zener model becomes Maxwell model.

One might derive that $G_2=\frac{\mu}{\lambda_1}-G$. To maintain physical adequacy, this spring coefficient should be positive and, thus, the restriction of Zener model is $\lambda_1<\frac{\mu}{G}$.

Dividing Eq. (8) by r and integrating the resulting equation from R to ∞, one can get:

$$\int_R^\infty\frac{\tau_{rr}+\lambda_1\dot{\tau_{rr}}}{r}dr=\int_R^\infty\frac{2G\gamma_{rr}+2\mu\dot{\gamma_{rr}}}{r} \tag{9}$$

We can then calculate:

$$\int_R^\infty\frac{2G\gamma_{rr}+2\mu\dot{\gamma_{rr}}}{r}=\frac{1}{3}\left(-\frac{4G}{3R^3}(R^3-R_0^3)-4\mu\frac{\dot{R}}{R}\right) \tag{10}$$

By introducing a new variable $q=\int_R^\infty\frac{\tau_{rr}(r,t)}{r}dr$, Eq. (9) becomes:

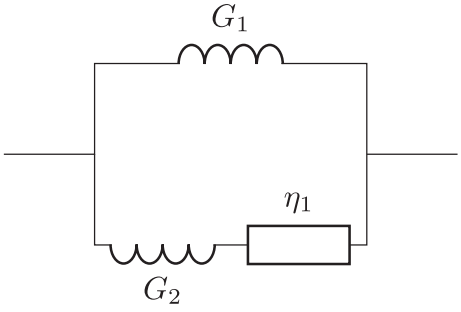

Fig. 1. Schematic of the Zener model.

$$q + \lambda_1\dot{q} + \lambda_1\frac{\dot{R}\tau_{rr}|_R}{R} = \frac{1}{3}\left(-\frac{4G}{3R^3}(R^3-R_0^3)-4\mu\frac{\dot{R}}{R}\right) \tag{11}$$

By evaluating Eq. (11) at $r = R$, an additional equation for $\tau_{rr}|_R$ is obtained as

$$\tau_{rr}|_R + \lambda_1\dot{\tau_{rr}}|_R = -\frac{4G}{3}\left(1-\frac{R_0^3}{R^3}\right)-4\mu\frac{\dot{R}}{R} \tag{12}$$

Thus, Zener model can be coupled with any cavitation model by adding two differential equations, namely Eqs. (11) and (12), and including the variables q and $\tau_{rr}|_R$ as follows:

$$\rho h(r) + \int_R^\infty\left(\frac{\partial\tau_{rr}}{\partial r} + \frac{3\tau_{rr}}{r}\right)dr = \rho h(r)-\tau_{rr}|_R + 3q \tag{13}$$

4. Gilmore-Akulichev-Zener model

To study bubble dynamics in a soft tissue (viscoelastic medium), authors propose to employ the combination of Gilmore-Akulichev's equation and Zener viscoelastic model. Gilmore-Akulichev model is the best cavitation model to simulate bubble collapse process (since it is observed in HIFU studies with continuous driving pulse). Zener viscoelastic model is considered to be suitable for soft tissue modeling, accounting for both essential soft tissue features: creep recovery and stress relaxation [34,44]. Eqs. (15)–(19) constitute the complete model to be employed in this study:

$$R\ddot{R}\left(1-\frac{\dot{R}}{C}\right) + \frac{3}{2}\dot{R}^2\left(1-\frac{\dot{R}}{3C}\right)= \tag{14}$$

$$\left(1 + \frac{\dot{R}}{C}\right)\left(H-\frac{\tau_{rr}|_R}{\rho_L} + \frac{3q}{\rho}\right)+$$
$$\frac{R}{C}\left(\dot{H}\left(1-\frac{\dot{R}}{C}\right)-\frac{1}{\rho_L}\frac{d}{dt}\tau_{rr}\Big|_R + \frac{1}{\rho_L}\frac{d}{dt}(3q)\right), \tag{15}$$

$$H = \frac{1}{\rho}\frac{n}{n-1}(p_0 + p_i(t) + B)\left(\left(\frac{\left(\left(p_0 + \frac{2S}{R_0}\right)\left(\frac{R_0}{R}\right)^{3\gamma}-\frac{2S}{R} + \tau_{rr}\Big|_R\right) + B}{p_0 + p_i(t) + B}\right)^{\frac{n-1}{n}}-1\right), \tag{16}$$

$$C = c_\infty\left(\frac{\left(\left(p_0 + \frac{2S}{R_0}\right)\left(\frac{R_0}{R}\right)^{3\gamma}-\frac{2S}{R} + \tau_{rr}\Big|_R\right) + B}{p_0 + p_i(t) + B}\right)^{\frac{n-1}{2n}} \tag{17}$$

$$q + \lambda_1\dot{q} + \lambda_1\frac{\dot{R}\tau_{rr}|_R}{R} = \frac{1}{3}\left(-\frac{4G}{3R^3}(R^3-R_0^3)-4\mu\frac{\dot{R}}{R}\right) \tag{18}$$

$$\tau_{rr}|_R + \lambda_1\dot{\tau_{rr}}|_R = -\frac{4G}{3}\left(1-\frac{R_0^3}{R^3}\right)-4\mu\frac{\dot{R}}{R} \tag{19}$$

The above equations have been solved numerically through six-stage Runge-Kutta method. In our simulations, if not specified otherwise, $P_0 = 1.013{*}10^5$ Pa, $f = 10^6$ Hz, $\rho = 1060$ kg/m^3, $c = 1500$ ms^{-1}.

5. Acoustic model

Two most well known models of finite-amplitude nonlinear wave propagation are Khokhlov-Zabolotskaya-Kuznetsov (KZK) and Westervelt equations. Westervelt equation is a full wave equation. In the limiting case of directional sound beams, this equation can be transformed to KZK equation. Nonlinear Westervelt equation for ultrasound pressure p has the following form:

$$\nabla^2 p-\frac{1}{c_0^2}\frac{\partial^2 p}{\partial t^2} + \frac{\delta}{c_0^4}\frac{\partial^3 p}{\partial t^3} + \frac{\beta}{\rho_0 c_0^4}\frac{\partial^2 p}{\partial t^2} = 0, \tag{20}$$

it takes into account the effects of diffraction, absorption and nonlinearity. The first two terms in Eq. (20) correspond to the effects of diffraction, the third term is responsible for an ultrasound attenuation, and the last one describes a nonlinear propagation effect.

In case of linear wave propagation, the shape of the signal has a harmonic form $p = A{*}\sin(2\pi ft)$. If nonlinear propagation effects are taken into account, higher harmonics are generated, and wave form becomes distorted. Since the shape of the distorted wave depends on many parameters (including transducer shape, tissue properties) – in the present paper, for clarity sake, only linear acoustic model will be considered. Hereafter, the Eq. (20) will be transformed into:

$$\nabla^2 p-\frac{1}{c_0^2}\frac{\partial^2 p}{\partial t^2} + \frac{\delta}{c_0^4}\frac{\partial^3 p}{\partial t^3} = 0. \tag{21}$$

Although, nonlinear propagation effects and relaxation effects can be easily added to the model, as it was done in our previous papers [33,45]. The influence of nonlinear wave propagation effects on the bubble dynamics shall be a subject of the further studies.

6. Numerical simulations

6.1. Verification and validation

In order to justify the employed numerical scheme, some verification and validation studies were performed.

Analytical solutions for Rayleigh-Plesset model were presented in [46] for the pulse-free case and gas-filled bubble $\left(p_G\left(\frac{R_0}{R}\right)^{3\gamma}\right)$ case with a polytropic exponent $\gamma = 1.5$. In [46], Rayleigh-Plesset equation was solved analytically for a non-dimensional form of the equation with respect to the variables $u = \frac{R}{R_0}$ and $T = \frac{t}{\omega_0^{-1}}$ at the constant values of $\omega = \frac{3\gamma p_G}{\rho R_0^2}$ and $\beta = \frac{p_0}{p_G}$. The solution has the following form of Weierstrass elliptic function:

$$u = \frac{9C_1}{8}-\wp\left\{\frac{1}{\sqrt{6}}(\tau-\tau_0),g_2,g_3\right\}^{-\frac{2}{3}},\quad T = \int_0^\tau u^{\frac{5}{2}}(\zeta)d\zeta, \tag{22}$$

where C_1 is an integration constant that can be calculated from the initial conditions. In the above, $g_2 = 3\left(\frac{9C_1}{4}\right)^2$ and $g_3 = 2\beta-\left(\frac{9C_1}{4}\right)^3$ are the elliptic invariants, τ_0 is a constant that can be obtained as a solution of the equation $\wp\left(\frac{1}{\sqrt{6}}\tau_0,g_2,g_3\right) = 0$. Fig. 2a exhibits the comparison between the analytical and numerical solutions.

The widespread modeling test case of the bubble collapse that takes into account the viscosity effect at the interface between bubble and liquid was presented in [47]. Fig. 2b shows that the current solution agrees with that in [47]. In [47], modified Herring-Trilling model was used (modified Rayleigh-Plesset). Pulse was set in a one-period harmonic form $P(t) = -A\cos(2\pi\omega t)$.

Purposely, to ensure an adequate accuracy of the current numerical solution of the equation involving the viscoelastic model, the test case with Keller-Miksis and Zener model [44] was performed. Pulse was set as a constant step increase in pressure $A = 3.4$ MPa. Fig. 2c shows the comparison between the current solution and the one obtained in [44].

6.2. Comparison of models

All models taking into account the acoustic damping effect show a very good agreement as can be seen in Fig. 3a, whereas Rayleigh-Plesset's model behaves in a different way. Therefore, it can be concluded that the inclusion of acoustic damping is an essential step for getting a proper modeling of cavitation dynamics, since bubble oscillations can be damped significantly. Fig. 3b demonstrates Mach number comparison for the different models. An amplitude was set accordingly to the HIFU amplitude range (1 MPa–20 MPa). However, it can be seen that the majority of models are out of their applicability range (given in

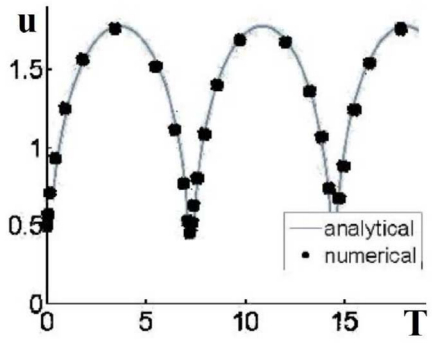

(a)

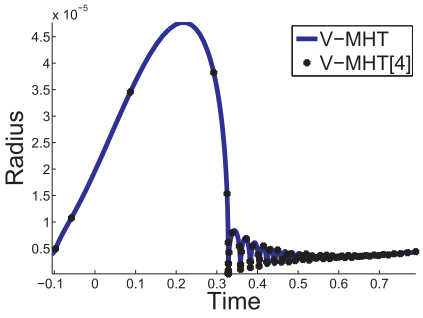

(b)

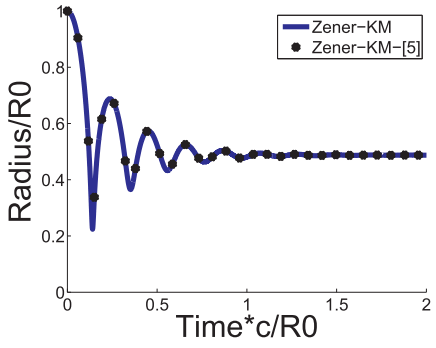

(c)

Fig. 2. (a) Agreement between numerical and analytical solutions (analytical solution – solid line, numerical solution – dashed line) is shown for the Rayleigh-Plesset model without pulse. Y – u, X – T. $u(0) = 1$, $u_t(0) = 0$, $C_1 = \frac{62}{135}$, $\beta = 1.05$. (b) Agreement between the current solution and that in [47] (current solution – solid line, [47] – dashed line) based on Modified Herring-Trilling equation (V-MHT). Y – bubble radius (m), X – time (sec) divided by period T = 38 μs. $A = 1.42{*}10^5$ Pa, $\omega = 26500$ Hz, $\sigma = 0.073$ kg/s^2, $\mu = 10^{-3}$ Pa s, $\rho = 10^3$ kg/m^3, $c = 1481$ ms^{-1}, $R_0 = 4{*}10^{-6}$. (c) Agreement between current solution and that in [44] (current solution – solid line, [44] – dashed line) based on Keller-Miksis model coupled with Zener viscoelastic model (Zener-KM). Y – bubble radius divided by R_0, X – $\frac{tc}{R_0}$. $A = 3.4{*}10^6$ Pa, $\sigma = 0.056$ kg/s^2, $\mu = 0.015$ Pa s (μ in Zener model), $G = 0.1{*}10^6$ Pa, $\lambda = 3{*}10^{-10}$ s, $\rho = 1060$ kg/m^3, $c = 1540$ ms^{-1}, $R_0 = 5{*}10^{-6}$.

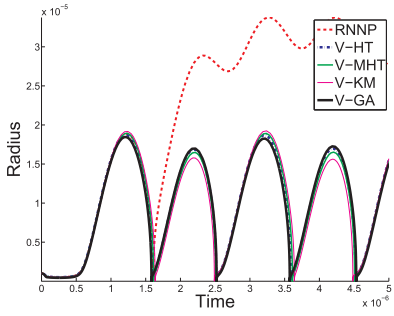

(a)

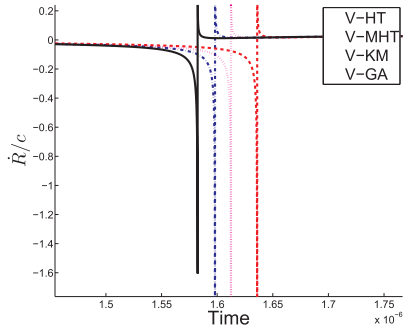

(b)

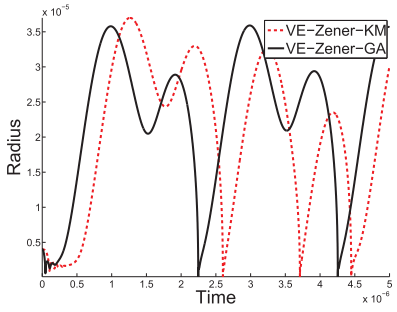

(c)

Fig. 3. (a) Comparison of Rayligh-Plesset's (RNNP), Herring-Trilling's (V-HT), Modified Herring-Trilling's (V-MHT), Keller-Miskis's (V-KM) and Gilmore-Akulichev's (V-GA) models with viscosity and surface tension boundary conditions, driving pressure is a continuous pulse. (b) Comparison of Mach number $\dot{R}/c$ for Herring-Trilling's (V-HT), Modified Herring-Trilling's (V-MHT), Keller-Miksis's (V-KM) and Gilmore-Akulichev's (V-GA) models with viscosity and surface tension boundary conditions. Simulation parameters: $A = 3{*}10^6$ Pa, $\mu = 0.015$ Pa s, $\sigma = 0.056$ kg/s^2, $R_0 = 1{*}10^{-6}$ m. Only Gilmore-Akulichev model can be applied at such high Mach numbers (Table 1). (c) Difference between Gilmore-Akulichev-Zener model and Keller-Miksis-Zener model, $A = 8{*}10^6$ Pa, $R_0 = 4{*}10^{-6}$ m.

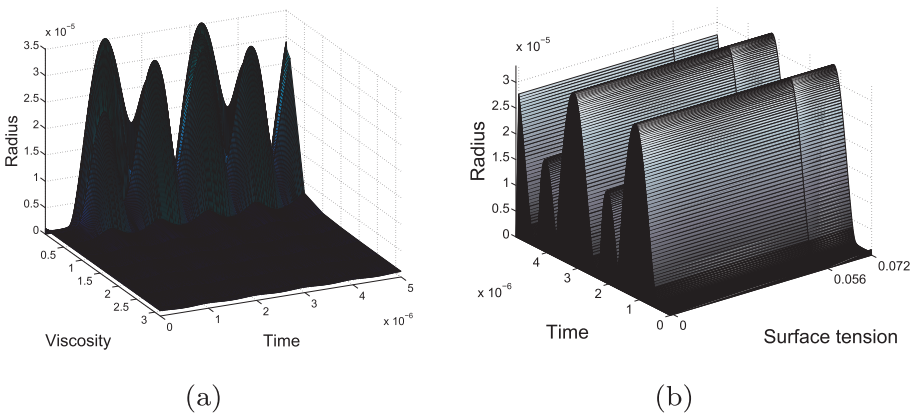

Fig. 4. (a) Viscosity effect for the Gilmore-Akulichev-Zener model. $A = 8{*}10^6$ Pa, $\sigma = 0.056$ kg/s^2, $R_0 = 1{*}10^{-6}$, $G = 0.1{*}10^6$ Pa, $\lambda = 3{*}10^{-9}$ s. (b) Surface tension effect for the Gilmore-Akulichev-Zener model. $A = 8{*}10^6$ Pa, $\mu = 0.015$ Pa s, $R_0 = 1{*}10^{-6}$, $G = 0.1{*}10^6$ Pa, $\lambda = 3{*}10^{-9}$ s.

Table 1): even the Keller-Miksis model's Mach number goes beyond its restriction value during bubble collapse. Whereas, Gilmore-Akulichev model still preserves Mach number less than 2.2 that proves the propriety of choice of this model for HIFU simulations. Viscosity and surface tension introduce damping to the system, thereby an inclusion of viscosity and surface tension boundary conditions into Gilmore-Akulichev model reduces Mach number. An increase in elasticity, as well, diminishes Mach number's values. Keller-Miksis-Zener model is quite often used in the literature for cavitation simulations. It shows very good agreement with Gilmore-Akulichev-Zener model at low and medium values of driving pulse amplitudes. However, with high amplitude values (where Keller-Miskis-Zener model becomes inapplicable because of high Mach numbers), the difference between these two models is significant and shows through occurrence of the additional bubble collapse (Fig. 3c). As it will be shown below, bubble collapse is very important, since its absence (or presence) can lead to the underestimation (or overestimation) of the values of temperature inside the bubble and amount of heat that is deposited in tissue.

6.3. Study of the effects of viscosity, surface tension, elasticity and relaxation time

The contribution of diverse effects was investigated by employing Gilmore-Akulichev-Zener model. For the soft tissue, viscosity was ranged from 0.001 Pa s to 3.15 Pa s (accordingly to [48]). In the previous studies, it was observed that viscosity accelerates bubble collapse and decreases bubble amplitude. This behavior was confirmed for the currently used model (Fig. 4a).

Variation of surface tension (Fig. 4b) does not demonstrate any strong impact on bubble dynamics: the diminution of the oscillation amplitude associated with surface tension is minimal (surface tension range for tissue was based on [26,49]).

As one might expect a raise of elasticity modulus G (Fig. 5) results in a dramatic restriction of oscillation and an amplitude, what goes in accordance with [50,44] (rigidity values range for tissue is set in agreement with [51,52,26,44]: 0–10 MPa). An increase in amplitude of the driving pulse emphasizes the elasticity effect.

The relaxation time effect is displayed on Fig. 6b. At low values of the relaxation time, when λ is much smaller than the period of the ultrasound wave (Fig. 6b: $\lambda = 10^{-9}$ s), there is a small difference between Zener and Kelvin-Voigt models ($\lambda = 0$). When relaxation time is close to the period of the ultrasound wave (Fig. 6b: 10^{-7} s$\leqslant \lambda < 10^{-6}$ s), the frequency of oscillations diminishes and the amplitude increases. With λ being approximately equal to the period of the wave (Fig. 6b: 10^{-6} s), the amplitude of oscillations reaches the maximum value. With further increase in relaxation time the amplitude starts decreasing. Since the elasticity damps the oscillations, larger elasticity values make bubble behavior more chaotic with respect to the relaxation time variation (Fig. 6a).

6.4. Temperature within the bubble

For the simulation of the temperature dynamics within the bubble, three approaches have been used. The first one is to assume the adiabatic equations of state for the bubble interior, meaning that there is no heat exchange between the bubble and exterior: $p_{gas} = p_G\left(\frac{R_0}{R}\right)^{3\gamma}$ and $T = T_0\left(\frac{R_0}{R}\right)^{3(\gamma-1)}$. The second approach consists in interpolating between isothermal and adiabatic behavior: it assumes heat exchange (isothermal motion) for most of the oscillation cycle, when bubble wall motion is relatively slow, and the adiabatic collapse, because during collapse, bubble motion is faster than the time scale of heat conduction [41,53]. This method was derived by Prosperetti [38] and is associated with employment of γ dependent on time that is meant to describe the interplay between isothermal and adiabatic regimes. For the second approach the following equations were used [41]:

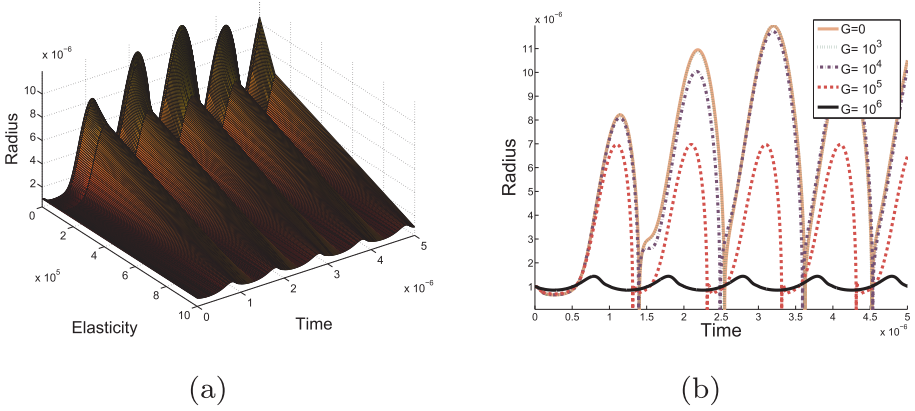

Fig. 5. Elasticity modulus G effect for the Gilmore-Akulichev-Zener model. $A = 1{*}10^6$ Pa, $\mu = 0.015$ Pa s, $\sigma = 0.056$ kg/s^2, $R_0 = 1{*}10^{-6}$, $\lambda = 3{*}10^{-9}$ s.

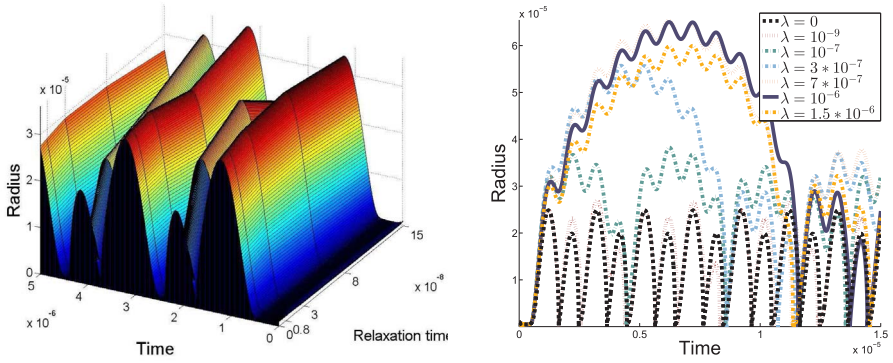

(a) (b)

Fig. 6. Relaxation time effect for the Gilmore-Akulichev-Zener model. (a) $A = 8{*}10^6$ Pa, $\mu = 0.015$ Pa s, $\sigma = 0.056$ kg/s^2, $R_0 = 1{*}10^{-6}$, $G = 0.1{*}10^6$ Pa. (b) $A = 5{*}10^6$ Pa, $\mu = 0.02$ Pa s, $\sigma = 0.056$ kg/s^2, $R_0 = 1{*}10^{-6}$, $G = 3{*}10^3$ Pa.

$$\dot{T} = -(\gamma(t,R)-1)\frac{3\dot{R}}{R}T - \chi_g(t)\frac{T-T_0}{R^2}, \tag{23}$$

$$\dot{p_{gas}} = -\gamma(t,R)\frac{3\dot{R}}{R}p_{gas}, \tag{24}$$

where χ_g is a thermal diffusivity. Other parameters were set according to the Enskog theory of gases [53,41].

Eqs. (23) and (24) were solved together with Eqs. (15)–(19). The coupling of the original model under the case of $\gamma \neq const$ results in a slightly different bubble and temperature dynamics comparing to the case of assuming solely $\gamma = const$ (Fig. 7). The order of temperature within the bubble in both cases was obtained to be near 10^4 (in K).

The third approach for the temperature inside calculation was proposed by [54,55]. In contrast with the above described methods, here, the inside temperature is a function of a distance from the center of the bubble. Following the approach of [56,57], the vapor mass transfer across the bubble surface is taken into account (bubble is considered to be a mixture of non-condensible gas and vapor). With assumption of spherical symmetry and ideal gas law for gas–vapor mixture, the temperature, pressure and vapor mass concentration within the bubble can be described by the following equations:

$$\frac{\gamma}{\gamma-1}\frac{p_{gas}}{T}\frac{\partial T}{\partial t} = -\frac{\gamma}{\gamma-1}\frac{p_{gas}}{T}U\frac{\partial T}{\partial r} + \frac{dp_{gas}}{dt} + K_g\left(\frac{2}{r}\frac{\partial T}{\partial r} + \frac{\partial^2 T}{\partial r^2}\right) \tag{25}$$

$$U = \frac{1}{\gamma p_{gas}}\left((\gamma-1)K_g\frac{\partial T}{\partial r} - \frac{r}{3}\frac{dp_{gas}}{dt}\right) \tag{26}$$

$$\frac{dp_{gas}}{dt} = \frac{3}{R}\left(-\gamma p_{gas}\dot{R} + (\gamma-1)K_g|_{r=R(t)}\frac{\partial T}{\partial r}\Big|_{r=R(t)} + \gamma R_v \dot{m}_v'' T|_{r=R(t)}\right) \tag{27}$$

$$\frac{\partial C}{\partial t} + u\frac{\partial C}{\partial r} = D\left(\frac{2}{r}\rho_m\frac{\partial C}{\partial r} + \frac{\partial \rho_m}{\partial r}\frac{\partial C}{\partial r} + \rho_m\frac{\partial^2 C}{\partial r^2}\right) \tag{28}$$

$$u = U + D\frac{R_v - R_g}{CR_v + (1-C)R_g}\frac{\partial C}{\partial r},$$

$$\rho_m = \frac{p_{gas}}{(CR_v + (1-C)R_g)T} \tag{29}$$

$$\dot{m}_v'' = D\frac{\rho_m|_{r=R(t)}}{1-C|_{r=R(t)}}\frac{\partial C}{\partial r}\Big|_{r=R(t)} \tag{30}$$

where $C = \frac{\rho_v}{\rho_m}$ is a vapor mass concentration, ρ_m a gas-vapor mixture density, r a distance from the center of the bubble, $\dot{m}_v''$ a vapor flux across the interface, K_g a thermal conductivity of the gas, D a diffusion coefficient ($D = 24.2{*}10^{-6}$ m^2/s), R_v a vapor gas constant, R_g a gas constant. Following [54], K_g can be approximated as a linear function of T: $K_g = AT + B$, where $A = 5.3{*}10^{-5}$ W/mK^2, $B = 1.17{*}10^{-2}$ W/mK are numerical values. Boundary conditions are as follows: $\frac{\partial T}{\partial r}\Big|_{r=0} = 0$, $T|_{r=R(t)} = T_{out}$, $\frac{\partial C}{\partial r}\Big|_{r=0} = 0$, $C|_{r=R(t)} = p_{sat}/\left(p_{gas}\frac{R_v}{R_g} - p_{sat}\left(\frac{R_v}{R_g}-1\right)\right)$, where p_{sat} denotes the saturated vapor pressure at the bubble wall and it is equal to $p_{sat} = p_{ref}e^{-\frac{T}{T_{ref}}}$ ($p_{ref} = 1.17{*}10^{11}$ Pa, $T_{ref} = 5200$ K [56]).

For the simplification of the given above formulation, during numerical simulation new variables were introduced: $y = \frac{r}{R(t)}$, $\tau = \int_{T_{out}}^{T} K(\theta)d\theta$. System of Eqs. (25)–(30) was solved together with Eqs. (15)–(19). Fig. 8 displays that obtained inside temperature and vapor concentration are not uniform within the bubble, what emphasizes the importance of diffusive processes. The highest value of the inside temperature is achieved at the center of the bubble and the lowest value turned out to be at the interface (this result goes in accordance with

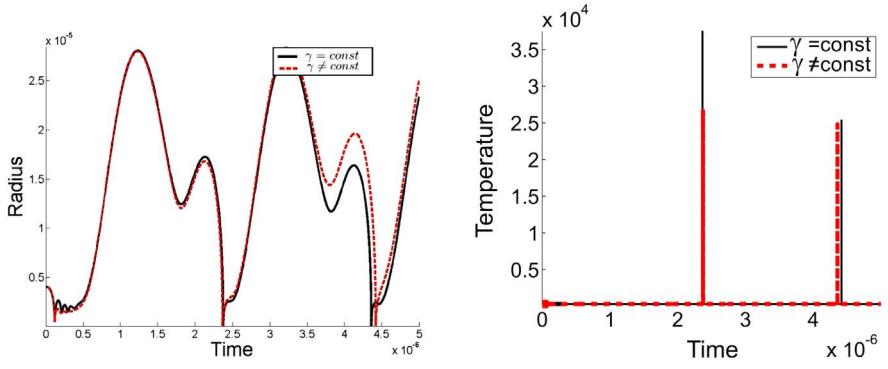

(a) (b)

Fig. 7. (a) Bubble dynamics for the case of assuming adiabatic behavior ($\gamma = const$, solid line) and adiabatic + isothermal behavior ($\gamma \neq const$, dashed line). (b) Temperature distribution (K) within the bubble assuming adiabatic behavior ($\gamma = const$, solid line) and adiabatic + isothermal behavior ($\gamma \neq const$, dashed line). $A = 5{*}10^6$ Pa, $\sigma = 0.056$ kg/s^2, $\mu = 0.015$ Pa s, $R_0 = 4{*}10^{-6}$, $G = 0.1{*}10^6$ Pa, $\lambda = 3{*}10^{-9}$ s.

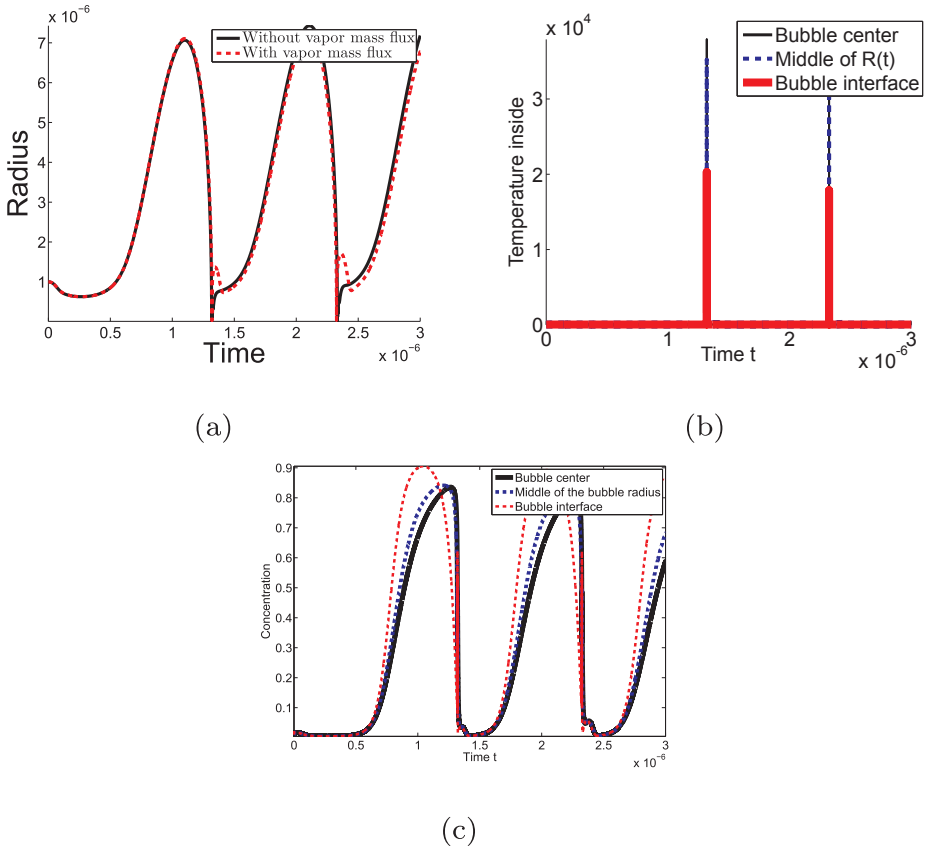

Fig. 8. Consideration of the interdiffusion of vapor and non-condensible gas inside the bubble. (a) Bubble dynamics for the Eqs. (25)–(30). (b) Temperature (K) within the bubble at the bubble center, at the middle of the bubble radius and at the bubble wall. (c) Vapor mass concentration at the bubble center, at the middle of the bubble radius and at the bubble wall. $A = 1{*}10^6$ Pa, $\sigma = 0.056$ kg/s^2, $\mu = 0.015$ Pa s, $R_0 = 1{*}10^{-6}$, $G = 0.1{*}10^6$ Pa, $\lambda = 3{*}10^{-9}$ s.

earlier studies [54,56]). The order of the obtained temperature values is the same that as for the two described above approaches. Regarding to the vapor concentration, at the bubble growing phase the vapor concentration at the bubble wall is highest (this effect also is confirmed by previous results [56]).

Influence of the tissue physical properties on the temperature inside the bubble was investigated. Fig. 9 demonstrates that elasticity and viscosity both reduce the values of temperature inside the bubble. Thus, the impact of these properties on the inside temperature resembles their influence on the radius of the bubble. The same conclusion can be made about the relaxation time: as for the radius of the bubble, the biggest temperature values are reached at the relaxation time values that are close to the period of the ultrasound wave (Fig. 9c). For different elasticity and initial radius values, bubble behavior can be more complex.

6.5. Heat deposition

According to [10] BHTE equation for tissue has the following form:

$$\rho c_t \frac{\partial T}{\partial t} = K_t \nabla^2 T - \omega_b c_b (T - T_\infty) + q_{ac} + q_{visc} + q_{rad}, \tag{31}$$

where ρ is a tissue density, c_t a specific heat, K a tissue thermal conductivity, ω_b a perfusion rate for the tissue cooling in capillary flows, T_∞ a far-field temperature in tissue. The ultrasound power deposition term q_{ac} is $q_{ac} = \frac{\alpha p^2}{\rho c}$ [58], where p is the driving pulse and α is a local acoustic absorption coefficient. The remaining terms q_{visc} and q_{rad} are cavitation terms responsible for viscous damping and absorption of the radiated pressure wave, respectively. Parameters in BHTE were set according to [58]: $c_t = 3600$ J/(kg K), $K = 0.512$ W/(m K), $\omega_b = 10$ kg/(m^3 s), $T_\infty = 310.15$ K, $\alpha = 9$ Np/m. Units of all heat source terms q_{ac}, q_{visc} and q_{rad} are W/m^3.

The spatial averaged power density that corresponds to viscous damping caused by cavitation is defined as follows:

$$q_{visc} = \frac{16\pi\mu R\dot{R}^2}{\frac{4}{3}\pi r'^3}, \tag{32}$$

where r' is the radius of the volume, upon which ultrasound power is deposited. This viscous cavitation energy appears at the bubble surface and is caused firstly by the viscous friction forces. Then it distributes in tissue through heat conduction.

When bubble collapses, the acoustic pulse is emitted in a form of a spherical wave. The acoustic emission data can be observed using passive cavitation detector [10]. During the pulse propagation, it is absorbed by the medium. The amplitude of spherical wave decreases with respect to the distance as $\frac{1}{r}e^{-\alpha r}$ (where α is an absorption coefficient).

To determine q_{rad}, firstly, we have to know the radiated pressure p_{rad} at the distance r from the bubble surface:

$$p_{rad} = \frac{\rho R}{r}(2\dot{R}^2 + R\ddot{R}) \tag{33}$$

The power deposited through a sphere with radius r', where acoustic emission is absorbed, has the following form:

$$D_{rad}^{abs} = 4\pi r^2 \frac{p_{rad}^2}{\rho c}(1 - e^{-2\alpha r'}), \tag{34}$$

where α is absorption coefficient.

By averaging by volume of the surrounding sphere $\frac{4}{3}\pi r'^3$, the term that corresponds to radiated pressure wave caused by bubble collapse is defined as follows [37]:

$$q_{rad} = \frac{3}{4\pi r'^3} D_{rad}^{abs} \tag{35}$$

Fig. 10a and b display that the heat deposition cavitation terms q_{rad} and q_{visc} reflect the bubble dynamics precisely. It is noted that their peaks might be observed only during the bubble collapse. Also, Fig. 10d demonstrates that the viscous emission is present all over the bubble

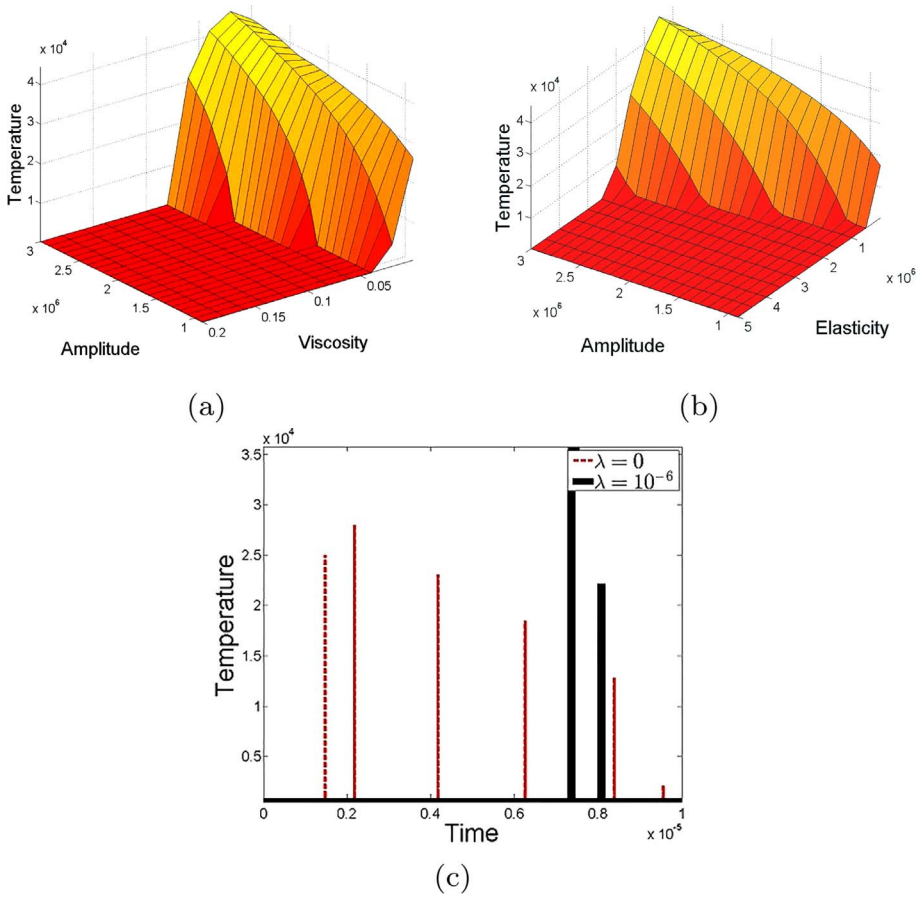

Fig. 9. (a) Viscosity effect on the temperature inside the bubble (K). $A = 8{*}10^6$ Pa, $\sigma = 0.056$ kg/s^2, $R_0 = 1{*}10^{-6}$, $G = 0.1{*}10^6$ Pa, $\lambda = 3{*}10^{-9}$ s. (b) Elasticity effect on the temperature inside the bubble (K). $A = 8{*}10^6$ Pa, $\sigma = 0.056$ kg/s^2, $R_0 = 1{*}10^{-6}$, $G = 0.1{*}10^6$ Pa, $\lambda = 3{*}10^{-9}$ s. (c) Relaxation time effect on the temperature inside the bubble (K). $A = 8{*}10^6$ Pa, $\sigma = 0.056$ kg/s^2, $R_0 = 1{*}10^{-6}$, $G = 0.1{*}10^6$ Pa, $\lambda = 3{*}10^{-9}$ s.

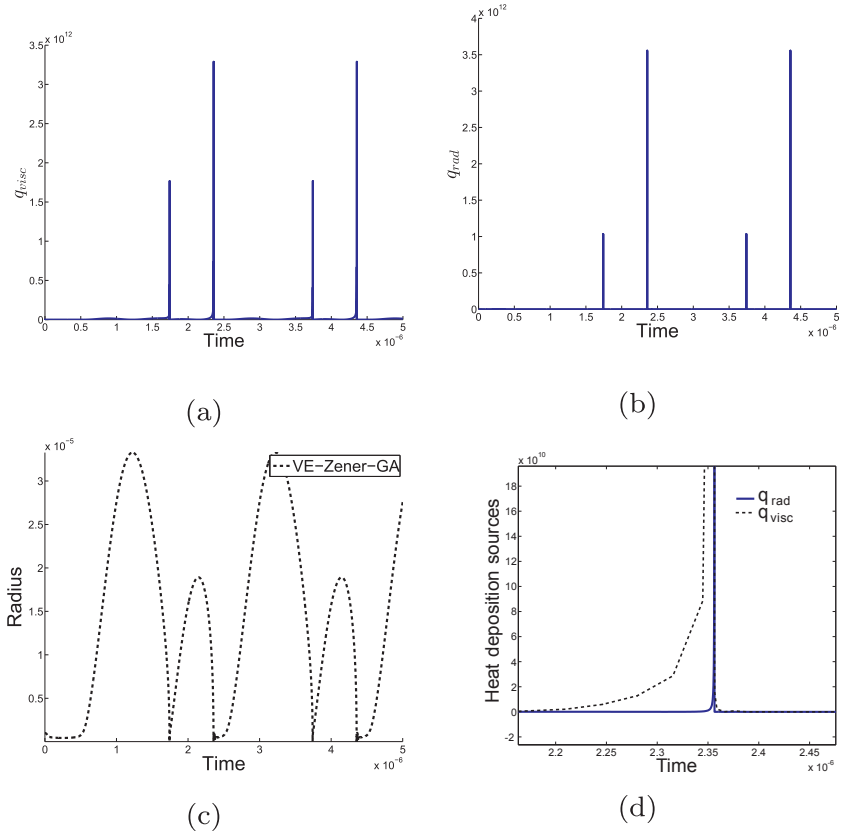

Fig. 10. Heat deposition sources. (a) Viscous damping term caused by cavitation q_{visc} (W/m^3); b) The term that corresponds to radiated pressure was caused by bubble collapse q_rad (W/m^3); (c) The corresponding bubble dynamics. d) Enlarged collapsing moment for both heat sources. $A = 8{*}10^6$ Pa,$\sigma = 0.056$ kg/s^2,$R_0 = 1{*}10^{-6}$,$G = 0.1{*}10^6$ Pa,$\lambda = 3{*}10^{-9}$ s,$r' = 0.1mm$.

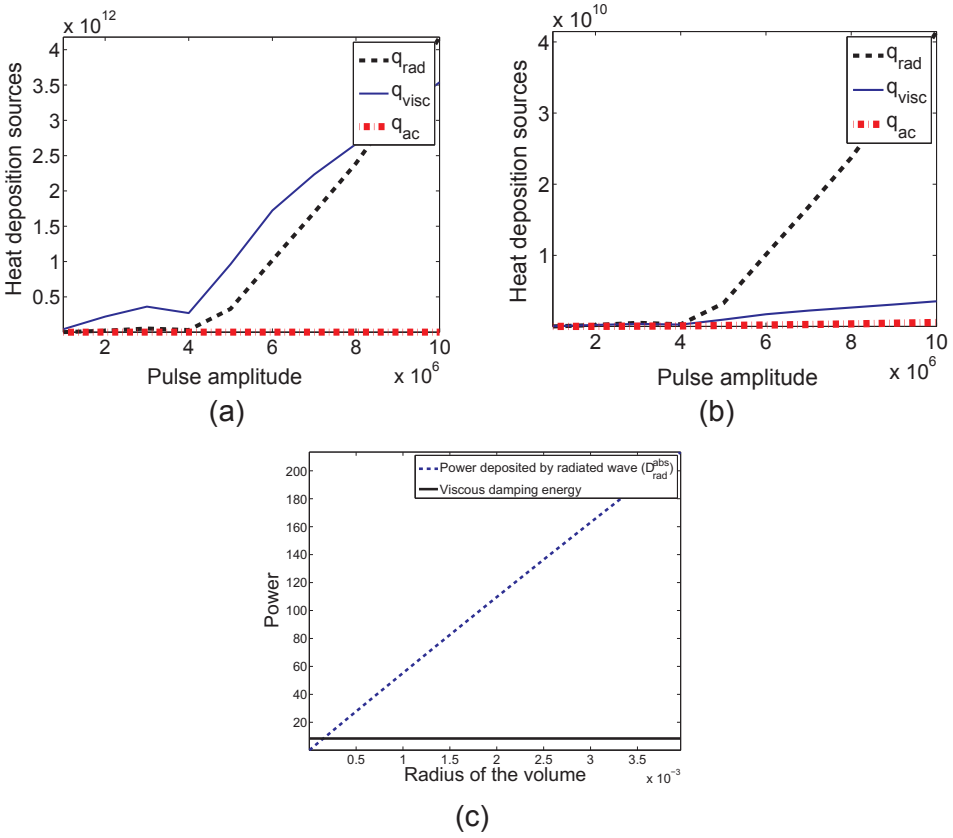

Fig. 11. The comparison of contribution of heat sources considering their maximum values: cavitation terms q_{rad},q_{visc} and acoustic term q_{ac} (W/m^3). (a) Surrounding volume radius $r' = 0.1$ mm; (b) Surrounding volume radius $r' = 1$ mm. (c) Deposited heat power corresponding to q_{rad} and q_{visc} as function of r' (not spatial averaged, W). Simulation parameters: A= $3*10^6$ Pa, $\sigma = 0.056$ kg/s^2, $R_0 = 4*10^{-6}$, $G = 0.1*10^6$ Pa, $\lambda = 3*10^{-9}$ s.

oscillation cycle, whereas the radiation wave appears at the moment of bubble collapse.

At low driving pressure amplitude, the maximum values achieved by q_{visc} are bigger than ones that are reached by q_{rad}. However, at high amplitudes (in case of HIFU), the situation changes: q_{rad} also becomes the essential bubble-related heating mechanism. Fig. 11a and b exhibit that maximum values that are achieved by both cavitation heat sources over dominate acoustic term q_{ac}.

As expected, the values of the radiation term q_{rad} and viscous damping term q_{visc} decrease with the increase of the radius r' (the heat deposition in tissue is investigated in the sphere of radius r' that surrounds oscillating bubble). This results in the situation that if the bubble surrounding volume is tight, maximum values of cavitation heat sources are comparable to each other and they both dominate the acoustic term significantly (Fig. 11a). Whereas in a case of large volume, acoustic term becomes more noticeable (Fig. 11b).

On Fig. 11c, the total heat power is represented without spatial averaging. It can be seen that viscous damping power is now independent of r'. Fig. 11c shows that with an increase in radius r', the amount of the absorbed energy that was radiated by bubble collapse enlarges. In this case, the difference between the radiation power and the viscous damping power can rise up to 20 times. From Fig. 11c, it can be concluded that, generally speaking, r' can be chosen differently for both heat cavitation terms: for q_{visc},r' should be set close to the bubble surface (since it is caused by forces acting at the bubble surface), whereas for q_{rad},r' should represent larger volume.

Diverse physical tissue properties have influence on the amount of heat deposition caused by cavitation and were investigated. As it was clear from the expression for the viscous damping cavitation term: q_{visc} increases with the increase of the viscosity. The elasticity influence was not obvious from the definition of the cavitation heat sources. However, from the previous analysis of the bubble dynamics one might expect that elasticity may lead to the diminution of the deposited heat values. This tendency can be observed for both cavitation heat sources on Fig. 12. The surface tension parameter did not display a very noticeable contribution for the heat deposition values within the HIFU amplitude

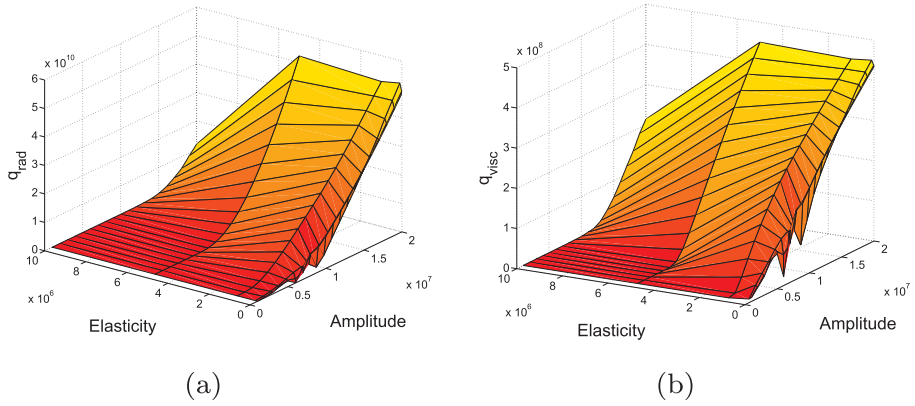

Fig. 12. Elasticity effect on the heat deposition induced by cavitation. (a) The term that corresponds to radiated pressure wave caused by bubble collapse q_{rad}. (b) Viscous damping term caused by cavitation q_{visc}. A= $4*10^6$ Pa, $\sigma = 0.056$ kg/s^2, $R_0 = 1*10^{-6}$, $G = 0.1*10^6$ Pa, $\lambda = 3*10^{-9}$ s, $r' = 1$ mm.

range. Less predictable behavior can be observed for the dependency of power deposition terms on the relaxation time. The effect becomes pronounced, when the relaxation time is close to the period of the wave.

7. Conclusion

In the present work, the model for the bubble dynamics in soft tissue during high-intensity focused ultrasound was proposed. The proposed model can deal with high ultrasound pressures and high frequencies that appear in HIFU applications. For the description of bubble dynamics, Gilmore-Akulichev cavitation model is chosen for the following reasons. Firstly, it was revealed that the effect of acoustic damping appeared to be an integral part of the correct bubble dynamics, therefore, Rayleigh-Plesset model should not be considered as a good choice for a detailed cavitation simulation. Secondly, Gilmore-Akulichev model can deal with high Mach number that appears to take place during bubble collapse that is frequently observed in case of continuous driving pulse (in contrast to other cavitation models, such as Keller-Miksis, Herring-Trilling and modified Herring-Trilling, whose applicability range is more restricted).

For a soft tissue modeling, Zener viscoelastic model was preferred to other viscoelastic models, in as much as it is considered to be the simplest viscoelastic model that is capable of describing both creep recovery and stress relaxation of tissue (in contrast, with Maxwell and Kelvin-Voigt models). The proposed cavitation-viscoelastic coupled model is deemed to be an accurate model for the description of the bubble cavitation in viscoelastic medium such as a soft tissue driven by a harmonic pulse induced by HIFU.

Contribution of diverse effects was studied based on the Gilmore-Akulichev-Zener model. It was concluded that the elasticity, viscosity and relaxation time can affect the bubble curve significantly. Elasticity and viscosity can both damp oscillations and can, therefore, restrict an amplitude, whereas the relaxation time effect strongly depends on the period of the ultrasound wave.

Cavitation effect can strongly impact the temperature elevation during HIFU therapy. The temperature within the bubble was calculated (the comparison of the temperatures was shown for two cases: the one assuming only the adiabatic regime and the other one implementing the interpolation between the adiabatic and isothermal regimes). However, the difference was found to be not significant, thereby resulting in the same order of the obtained temperatures during the bubble collapse. The internal temperature of the bubble during collapse can reach up to several thousands degrees. Influence of the tissue properties and ultrasound radiation parameters on the inside temperature resembles their impact on the bubble radius.

The temperature distribution within the tissue can be described by the bioheat equation with two extra terms responsible for the cavitation. One term corresponds to the viscous damping, another one to the pressure wave radiated by bubble collapse. At high intensities, maximum values of both cavitation terms overdominate the acoustic term. Viscous damping term is mainly distributed close to the bubble surface, whereas the radiation power source can cause temperature increase in a region that is far away from the bubble surface. Chavrier et al. [40] experimentally showed that at the 1 mm distance from the bubble surface, temperature can increase up to 100° C.

In our previous studies, the three fields coupled mathematical model [33,45,59] has been developed for the modeling of temperature elevation in a patient specific liver geometry. The physical model takes into account the convective cooling in large blood vessel and the perfusion due to capillary flows. The effect of acoustic streaming is also taken into account. In the following studies, we are going to combine the developed three fields coupled model with the proposed in the current paper cavitation and bioheat models and further investigate, how cavitation effects can impact the temperature elevation in tissue.

8. Acknowledgement

This research was supported by the Ministry of Science and Technology, R.O.C., under the grant MOST-105-2221-E-400-005 and by National Health Research Institute's project BN-106-PP-08.

References

[1] T. Leighton, The Acoustic Bubble, Academic Press, 2012.
[2] L. Rayleigh, VIII. On the pressure developed in a liquid during the collapse of a spherical cavity, Lond., Edinburgh, Dublin Philos. Mag. J. Sci. 34 (1917) 94–98.
[3] M.S. Plesset, The dynamics of cavitation bubbles, J. Appl. Mech. 16 (1949) 277–282.
[4] D. Cosgrove, Ultrasound contrast agents: an overview, Eur. J. Radiol. 60 (2006) 324–330.
[5] R. Schlief, Ultrasound contrast agents, Curr. Opin. Radiol. 3 (1991) 198–207.
[6] Y.-F. Zhou, High intensity focused ultrasound in clinical tumor ablation, World J. Clin. Oncol. 2 (2011) 8.
[7] T. Leslie, J. Kennedy, High intensity focused ultrasound in the treatment of abdominal and gynaecological diseases, Int. J. Hyperthermia 23 (2007) 173–182.
[8] O. Al-Bataineh, J. Jenne, P. Huber, Clinical and future applications of high intensity focused ultrasound in cancer, Cancer Treat. Rev. 38 (2012) 346–353.
[9] M.A. Solovchuk, M. Thiriet, T.W. Sheu, Computational study of acoustic streaming and heating during acoustic hemostasis, Appl. Therm. Eng. (2017).
[10] C.C. Coussios, R.A. Roy, Applications of acoustics and cavitation to noninvasive therapy and drug delivery, Annu. Rev. Fluid Mech. 40 (2008) 395–420.
[11] M.A. Solovchuk, S.C. Hwang, H. Chang, M. Thiriet, T.W. Sheu, Temperature elevation by hifu in ex vivo porcine muscle: mri measurement and simulation study, Med. Phys. 41 (2014).
[12] H.H. Pennes, Analysis of tissue and arterial blood temperatures in the resting human forearm, J. Appl. Physiol. 1 (1948) 93–122.
[13] T.W. Sheu, M.A. Solovchuk, A.W. Chen, M. Thiriet, On an acoustics–thermal–fluid coupling model for the prediction of temperature elevation in liver tumor, Int. J. Heat Mass Transfer 54 (2011) 4117–4126.
[14] A.J. Coleman, J.E. Saunders, L.A. Crum, M. Dyson, Acoustic cavitation generated by an extracorporeal shockwave lithotripter, Ultrasound Med. Biol. 13 (1987) 69–76.
[15] C.C. Church, A theoretical study of cavitation generated by an extracorporeal shock wave lithotripter, J. Acoust. Soc. Am. 86 (1989) 215–227.
[16] Z. Xu, J.B. Fowlkes, E.D. Rothman, A.M. Levin, C.A. Cain, Controlled ultrasound tissue erosion: the role of dynamic interaction between insonation and microbubble activity, J. Acoust. Soc. Am. 117 (2005) 424–435.
[17] A.D. Maxwell, C.A. Cain, A.P. Duryea, L. Yuan, H.S. Gurm, Z. Xu, Noninvasive thrombolysis using pulsed ultrasound cavitation therapy–histotripsy, Ultrasound Med. Biol. 35 (2009) 1982–1994.
[18] L. Trilling, The collapse and rebound of a gas bubble, J. Appl. Phys. 23 (1952) 14–17.
[19] C. Herring, Theory of the Pulsations of the Gas Bubble Produced by an Underwater Explosion, Columbia Univ, Division of National Defense Research, 1941.
[20] J.B. Keller, M. Miksis, Bubble oscillations of large amplitude, J. Acoust. Soc. Am. 68 (1980) 628–633.
[21] J.B. Keller, I.I. Kolodner, Damping of underwater explosion bubble oscillations, J. Appl. Phys. 27 (1956) 1152–1161.
[22] D. Epstein, J.B. Keller, Expansion and contraction of planar, cylindrical, and spherical underwater gas bubbles, J. Acoust. Soc. Am. 52 (1972) 975–980.
[23] L. Hoff, Acoustic Characterization of Contrast Agents for Medical Ultrasound Imaging, Springer Science & Business Media, 2001.
[24] F.R. Gilmore, The growth or collapse of a spherical bubble in a viscous compressible liquid (1952).
[25] I. Tanasawa, W.-J. Yang, Dynamic behaviour of a gas bubble in viscoelastic liquids, J. Appl. Phys. 41 (1970) 4526–4531.
[26] X. Yang, C.C. Church, A model for the dynamics of gas bubbles in soft tissue, J. Acoust. Soc. Am. 118 (2005) 3595–3606.
[27] R. Gaudron, M. Warnez, E. Johnsen, Bubble dynamics in a viscoelastic medium with nonlinear elasticity, J. Fluid Mech. 766 (2015) 54–75.
[28] P. Movahed, W. Kreider, A.D. Maxwell, S.B. Hutchens, J.B. Freund, Cavitation-induced damage of soft materials by focused ultrasound bursts: a fracture-based bubble dynamics model, J. Acoust. Soc. Am. 140 (2016) 1374–1386.
[29] M. Warnez, E. Johnsen, Numerical modeling of bubble dynamics in viscoelastic media with relaxation, Phys. Fluids 27 (2015) 063103.
[30] E. Brujan, Cavitation in Non-Newtonian Fluids: With Biomedical and Bioengineering Applications, Springer Science & Business Media, 2010.
[31] E. Brujan, The equation of bubble dynamics in a compressible linear viscoelastic liquid, Fluid Dyn. Res. 29 (2001) 287–294.
[32] S. Catheline, J.-L. Gennisson, G. Delon, M. Fink, R. Sinkus, S. Abouelkaram, J. Culioli, Measurement of viscoelastic properties of homogeneous soft solid using transient elastography: an inverse problem approach, J. Acoust. Soc. Am. 116 (2004) 3734–3741.
[33] M. Solovchuk, T.W. Sheu, M. Thiriet, Simulation of nonlinear westervelt equation for the investigation of acoustic streaming and nonlinear propagation effects, J. Acoust. Soc. Am. 134 (2013) 3931–3942.
[34] Y. Zheng, X. Chen, A. Yao, H. Lin, Y. Shen, Y. Zhu, M. Lu, T. Wang, S. Chen, Shear wave propagation in soft tissue and ultrasound vibrometry, Wave Propagation Theories and Applications, InTech, 2013.

[35] V. Suomi, Y. Han, E. Konofagou, R.O. Cleveland, The effect of temperature dependent tissue parameters on acoustic radiation force induced displacements, Phys. Med. Biol. 61 (2016) 7427.
[36] M. Orosz, G. Molnarka, E. Monos, Curve fitting methods and mechanical models for identification of viscoelastic parameters of vascular wall-a comparative study, Med. Sci. Monit. 3 (1997) MT599–MT604.
[37] C.H. Farny, R.G. Holt, R.A. Roy, The correlation between bubble-enhanced hifu heating and cavitation power, IEEE Trans. Biomed. Eng. 57 (2010) 175–184.
[38] A. Prosperetti, Thermal effects and damping mechanisms in the forced radial oscillations of gas bubbles in liquids, J. Acoust. Soc. Am. 61 (1977) 17–27.
[39] R. Holt, R. Roy, Bubble dynamics in therapeutic ultrasound, Bubble Part. Dyn. Acoust. Fields: Modern Trends Appl. (2005) 108–229.
[40] F. Chavrier, J. Chapelon, A. Gelet, D. Cathignol, Modeling of high-intensity focused ultrasound-induced lesions in the presence of cavitation bubbles, J. Acoust. Soc. Am. 108 (2000) 432–440.
[41] M.P. Brenner, S. Hilgenfeldt, D. Lohse, Single-bubble sonoluminescence, Rev. Mod. Phys. 74 (2002) 425.
[42] A. Prosperetti, Bubble phenomena in sound fields: part one, Ultrasonics 22 (1984) 69–77.
[43] K. Vokurka, Comparison of rayleigh's, herring's, and gilmore's models of gas bubbles, Acta Acustica United Acustica 59 (1986) 214–219.
[44] C. Hua, E. Johnsen, Nonlinear oscillations following the rayleigh collapse of a gas bubble in a linear viscoelastic (tissue-like) medium, Phys. Fluids 25 (2013) 083101.
[45] M. Solovchuk, T.W.-H. Sheu, M. Thiriet, Multiphysics modeling of liver tumor ablation by high intensity focused ultrasound, Commun. Comput. Phys. 18 (2015) 1050–1071.
[46] N.A. Kudryashov, D.I. Sinelshchikov, Analytical solutions of the rayleigh equation for empty and gas-filled bubble, J. Phys. A: Math. Theor. 47 (2014) 405202.
[47] S. Hilgenfeldt, M.P. Brenner, S. Grossmann, D. Lohse, Analysis of rayleigh–plesset dynamics for sonoluminescing bubbles, J. Fluid Mech. 365 (1998) 171–204.
[48] R.G. Holt, R.A. Roy, Measurements of bubble-enhanced heating from focused, mhz-frequency ultrasound in a tissue-mimicking material, Ultrasound Med. Biol. 27 (2001) 1399–1412.
[49] E. Vlaisavljevich, K.-W. Lin, A. Maxwell, M.T. Warnez, L. Mancia, R. Singh, A.J. Putnam, B. Fowlkes, E. Johnsen, C. Cain, et al., Effects of ultrasound frequency and tissue stiffness on the histotripsy intrinsic threshold for cavitation, Ultrasound Med. Biol. 41 (2015) 1651–1667.
[50] C.C. Church, X. Yang, The mechanical index and cavitation in tissue, J. Acoust. Soc. Am. 117 (2005) 2530–2530.
[51] E.L. Madsen, H.J. Sathoff, J.A. Zagzebski, Ultrasonic shear wave properties of soft tissues and tissuelike materials, J. Acoust. Soc. Am. 74 (1983) 1346–1355.
[52] P.N. Wells, H.-D. Liang, Medical ultrasound: imaging of soft tissue strain and elasticity, J. R. Soc. Interface 8 (2011) 1521–1549.
[53] S. Hilgenfeldt, S. Grossmann, D. Lohse, Sonoluminescence light emission, Phys. Fluids 11 (1999) 1318–1330.
[54] A. Prosperetti, L.A. Crum, K.W. Commander, Nonlinear bubble dynamics, J. Acoust. Soc. Am. 83 (1988) 502–514.
[55] A. Prosperetti, The thermal behaviour of oscillating gas bubbles, J. Fluid Mech. 222 (1991) 587–616.
[56] A.T. Preston, Modeling Heat and Mass Transfer in Bubbly Cavitating Flows and Shock Waves in Cavitating Nozzles (Ph.D. thesis), California Institute of Technology, 2004.
[57] C. Barajas, E. Johnsen, The effects of heat and mass diffusion on freely oscillating bubbles in a viscoelastic, tissue-like medium, J. Acoust. Soc. Am. 141 (2017) 908–918.
[58] M.A. Solovchuk, T.W. Sheu, M. Thiriet, W.-L. Lin, On a computational study for investigating acoustic streaming and heating during focused ultrasound ablation of liver tumor, Appl. Therm. Eng. 56 (2013) 62–76.
[59] M.A. Solovchuk, T.W. Sheu, M. Thiriet, Image-based computational model for focused ultrasound ablation of liver tumor, J. Comput. Surgery 1 (2014) 4.